

A spatial climatology of North Atlantic hurricane intensity change

Erik Fraza* and James B. Elsner

Department of Geography, Florida State University, Tallahassee, FL, USA

ABSTRACT: A spatial analysis of intensity change has yet to be considered in hurricane climatology. Here we use a unique hourly interpolated version of the Atlantic hurricane dataset together with a novel spatial tessellation of the basin to examine the climatology of hurricane intensity change. We find that the frequency of hurricanes is highest across the central part of the basin, but regions of highest intensity are located farther south across the Caribbean. Standard errors of the mean intensities are largest in the regions adjacent to land. Highest mean intensification rates are found in the Gulf of Mexico and the Caribbean Sea, and the mean intensification is getting larger in the southeast portion of the basin. We find greater spatial coherency in intensification rates over the period from 1986 to 2011 compared with the period from 1967 to 1985. The reason for this change is unknown but it is likely due to improved surveillance technology. We also find that the statistical relationship between intensity and intensification is getting stronger and tighter and note that this might be associated with the implementation of the Dvorak Technique.

KEY WORDS hurricane; tropical cyclone; intensity; intensification; climatology

Received 6 May 2013; Revised 31 October 2013; Accepted 6 November 2013

1. Introduction

A hurricane is a warm-core non-frontal synoptic-scale cyclone, originating over tropical or subtropical waters, with organized deep convection and a closed surface wind circulation about a well-defined centre (NHC, 2013). Hurricane intensity as measured by the maximum sustained near-surface wind speed is the subject of considerable climatological and societal interest. Observed upward trends in the maximum intensity of the strongest hurricanes (Elsner *et al.*, 2008) are consistent with maximum potential intensity (MPI) theory, which gives an exact equation for the minimum sustainable central pressure of hurricanes (Emanuel, 1988). The spatial distribution of limiting intensity and its relationship with ocean temperature indicate a sensitivity of about $8 \text{ m s}^{-1} \text{ K}^{-1}$ for hurricanes over the North Atlantic (Elsner *et al.*, 2012). This sensitivity is not matched in tropical cyclones generated by general circulation models (GCMs) from 1981 to 2010 (Elsner *et al.*, 2013).

The change of intensity over time is also of interest, but climatological studies of intensification are less common. A climatological basin-wide study of the Atlantic was done by Balling and Cerveny (2006). They note that there is no significant trend in average intensification rates over the period 1970–2003. Most of the basin-wide intensification studies concern rapid intensification. Kaplan and DeMaria (2003) introduce an index to

predict rapid intensification of at least 25 kt in a 24 h period. Kaplan *et al.* (2010) improve the 2003 rapid intensification index by introducing some new predictors and improving others. Rozoff and Kossin (2011) develop a logistic regression model and a Bayesian probabilistic model that outperforms the rapid intensification index of Kaplan *et al.* (2010). Recently, Kishtawal *et al.* (2012) looked at changes in tropical cyclone intensification with basin-wide statistics using data since 1986. Lacking is a spatial climatology of intensity change.

Here we examine the spatial distribution of intensity change for hurricanes over the North Atlantic basin with the goal of achieving a better understanding of the relationship between intensity change and climate variability. This research is made possible by two recent innovations. First, we use a new 1-h interpolated and smoothed version of Atlantic hurricane data (or HURDAT) that provides intensification rates along each hurricane track (Elsner and Jagger, 2013). Second, we make use of a hexagonal tessellation of the basin (Elsner *et al.*, 2012). These two innovations together allow a spatial climatology of intensification.

This paper is outlined as follows. In Section 2 we describe our new version of the hurricane-track data including a summary of how the smoothing and interpolations were done. Here we also describe and explain the rationale behind our spatial grid for aggregating the track data. In Section 3 we present a spatial climatology of hurricane frequency, intensity, and intensity change over the period 1986–2011. We map the frequency of hurricanes, the number of hurricane hours, the average

* Correspondence to: E. Fraza, Department of Geography, Florida State University, Tallahassee, FL 32306, USA. E-mail: ef10c@fsu.edu

intensity, and the average intensity change. For the averages, we also map the corresponding standard errors. In Section 4 we map the maximum decay and maximum intensification rates, and examine Moran's *I* using two different time periods. In Section 5 we examine the relationship between average intensity and intensification using the same two time periods. In Section 6 we provide a summary of the main findings.

2. Tracks and grids

2.1. Best-track data

The data used in this study originate from an analysis by the US National Oceanic and Atmospheric Administration (NOAA) and National Hurricane Center (NHC) operational meteorologists of all known tropical cyclones from 1967 to 2011. The HURDAT dataset includes estimates of the hurricane's centre position and intensity (Jarvinen *et al.*, 1984). Centre location (fix) is given in geographic coordinates (in tenths of degrees) and the intensity, representing the 1-min near-surface (~ 10 m) wind speed, is given in knots ($1 \text{ kt} = .5144 \text{ m s}^{-1}$). The minimum central pressure, where available, is given in millibars ($1 \text{ mb} = 1 \text{ hPa}$).

The data are provided in six-hourly intervals starting at 00 UTC (Universal Time Coordinate). Information related to landfall time, local wind speeds, damages, deaths as well as cyclone size is available but not used here. Here we use a version of the dataset that contain all known hurricanes through the 2011 season and downloaded from www.nhc.noaa.gov/pastall.shtml#hurdat.

2.2. Time rate of change

Value is added to these data by computing the time rate of change of intensity and then interpolating the values to 1-h intervals (Elsner and Jagger, 2013). The rate of change is estimated with a numerical derivative. This is done with the Savitzky-Golay smoothing filter (Savitzky and Golay, 1964). The filter, specifically designed for calculating derivatives, preserves the maximum and minimum cyclone intensities, whereas moving averages damp the extremes and simple finite differencing schemes have larger errors.

The smoothed value of intensity along the track is estimated using a local polynomial regression of degree three on a window of six values (including three locations before and two after). This gives a window width of 1.5 days. A third-degree polynomial captures most of the fluctuation in cyclone intensity without over-fitting to the random variations and consistent with the 2.6 m s^{-1} precision of the best-track wind speeds.

The HURDAT values are recorded every six hours but are interpolated in the new dataset to every 1 h. The higher temporal resolution allows for a finer spatial resolution. The interpolation is done with splines. The spline interpolation preserves the values at the regular 6-h times and uses a piecewise polynomial to obtain values in

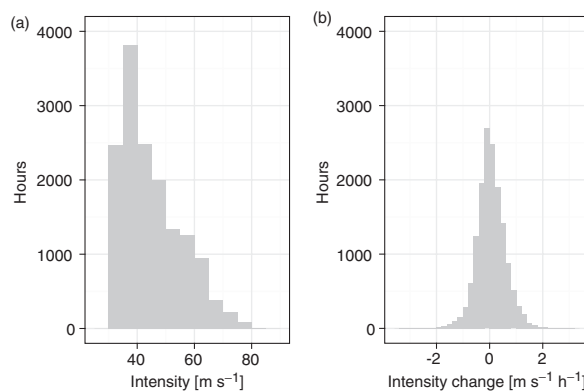


Figure 1. Hurricane intensity and intensity change. (a) Histogram of hurricane intensity in 5 m s^{-1} intervals. (b) Histogram of hurricane intensity change in $0.2 \text{ m s}^{-1} \text{ h}^{-1}$ intervals. Data are over the period 1986–2011.

between these times. The splines are done using spherical geometry to locate the centre of the hurricanes. Details are given in Elsner and Jagger (2013).

Our interest here is the spatial distribution of the time rate of intensity change. We limit our study to tropical cyclones at hurricane intensity (33 m s^{-1}) and above. This is because hurricanes cause a majority of the damage associated with tropical cyclones, especially those caused by wind. Because our goal is a climatology of intensification, hurricane intensification is more of a concern than tropical storm intensification. We restrict the data further to the portion of the hurricane track where the centre fix is over water. The climatology of hurricane decay (and sometimes intensification) over land areas is beyond the scope of the present work.

2.3. Intensity and intensity change

Figure 1 shows histograms of basin-wide hourly intensity and intensity change for the North Atlantic. Intensities are binned in 5 m s^{-1} intervals starting at 30 m s^{-1} . The number of hours is shown on the ordinate. The average intensity is 45 m s^{-1} , but the distribution is skewed with the lower intensity bins having the most hours. Intensities above 70 m s^{-1} account for less than 2.2% of all hurricane hours.

Intensity changes are binned in $0.2 \text{ m s}^{-1} \text{ h}^{-1}$ intervals centred on zero. The distribution is peaked near zero. The -0.2 to $0 \text{ m s}^{-1} \text{ h}^{-1}$ interval has the most hurricane hours, but the mean and median intensity changes are $+0.054$ and $+0.0059 \text{ m s}^{-1} \text{ h}^{-1}$, respectively. The vast majority (99.6%) of the hours have intensity changes between $\pm 2 \text{ m s}^{-1} \text{ h}^{-1}$.

2.4. Spatial grids

Here we adopt the spatial framework developed by Elsner *et al.* (2012). The framework consists of a tessellation of the hurricane basin using equal-area hexagon grids on a Lambert conformal conic projection. The secants are the 23°N and 38°N parallels and the tessellation is centred on 60°W meridian. The grid is constructed by covering

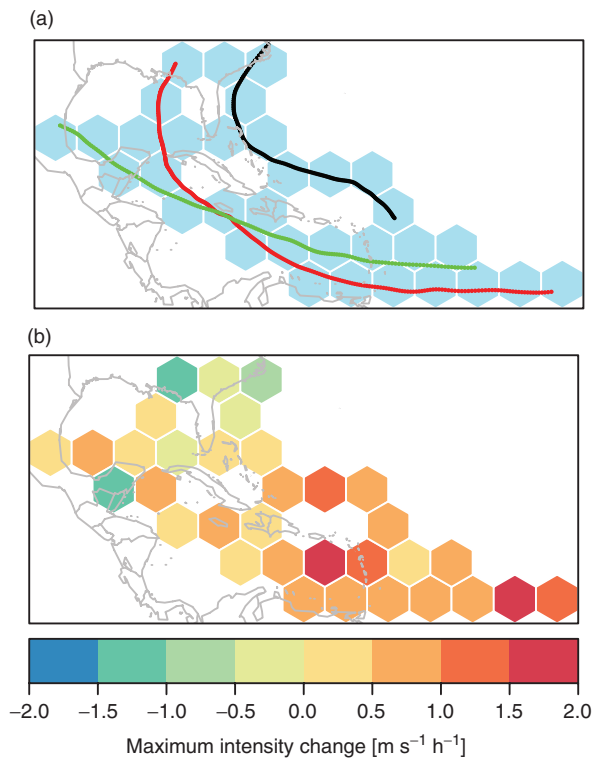


Figure 2. Tracks and maximum intensity change. (a) The tracks and corresponding grids from Hurricane Floyd (1999; black), Ivan (2004; red) and Dean (2007; green). (b) Maximum 1-h intensity change.

the domain, determined by the spatial extent of the centre fixes, with hexagons.

Figure 2(a) displays three sample storms: Floyd (1999), Ivan (2004), and Dean (2007) and the corresponding grids. Only grids having at least one centre fix with intensities at or above hurricane intensity are included. Figure 2(b) shows the per hexagon maximum intensity change over all hurricane hours. For these three hurricanes largest intensity changes occur over the eastern Caribbean Sea eastward into the central Atlantic.

3. Frequency, intensity, and intensity change

Here we use the aforementioned spatial framework together with the hourly interpolated best tracks from the period 1986–2011 to present a spatial climatology of frequency, intensity, and intensity change. Hurricane frequency is examined using the per grid number of hurricane hours and the per grid number of hurricanes. Hurricane intensity and intensity change are examined using grid averages. Hurricane hours is the number of centre fixes inside the hexagon across all hurricanes.

The spatial distribution of hurricane frequency is shown in Figure 3. The patterns are similar, showing the largest risk across the western part of the basin generally north and east of the Bahamas. The region having the greatest number of hurricanes is shifted slightly northward relative to the region with the highest number of hurricane hours. This results in part from the

fact that hurricanes farther south tend to move slower. The spatial variability in the number of hurricane hours per grid is quite large over the western Caribbean Sea and across the Gulf of Mexico with several grids having between 50 and 75 h and with one grid having between 275 and 300 h.

The spatial distribution of hurricane intensity is shown in Figure 4. On average grids across the central and western Caribbean have the highest hurricane intensities. Climatologically this is where the ocean is hottest and ocean heat content is highest. In contrast, in the region of maximum hurricane occurrence north of the Bahamas, average hurricane intensity is considerably less.

The high hurricane frequency off the East Coast of the United States is the result of being northwest of the main development region (central Atlantic through the Caribbean) and steering currents. Hurricanes that form to the south and east get steered northwestward typically around the Bermuda High, which tends to be located near or to the northeast of Bermuda.

We estimate our uncertainty on all our estimates using standard error. A larger value of standard error indicates greater uncertainty. Standard errors in Figure 4 tend to be largest in areas with higher average intensity and in areas near land.

The spatial distribution of intensity change is shown in Figure 5. Most grids across the southern half of the basin have a positive mean intensity change while most grids across the northern half of the basin have a negative mean intensity change. The largest average intensity changes are over the Caribbean, Gulf of Mexico, and the eastern Atlantic. Standard errors tend to be smallest in regions away from land.

The average intensity change shown in Figure 5 is over all hours regardless of whether the hurricane is weakening or intensifying. Here we consider the spatial pattern of intensity change separately for weakening and intensifying hurricanes. Figure 6 shows the per hexagon maximum decay (decreasing intensity) and per hexagon maximum intensification (increasing intensity).

Regions of maximum decay are noted over the western North Atlantic and near land areas (Figure 6(a)). This includes grids on the margins of the Caribbean Sea and the Gulf of Mexico. Maximum decay rates are also relatively high over the eastern Caribbean and northeast of Puerto Rico. Maximum decay rates are relatively low across the west central Gulf of Mexico and in the grid that includes Jamaica. The western North Atlantic away from the coast that includes Bermuda is also a region where maximum decay rates are relatively low.

Regions of maximum intensification are noted over the Caribbean Sea northwestward into the Gulf of Mexico (Figure 6(b)). Another region of relatively high maximum intensification occurs from the eastern and central North Atlantic northwestward towards Bermuda. Weakest intensification rates occur in grids over the northwestern part of the basin. There is also a region east of the Lesser Antilles that stretches northeastward and

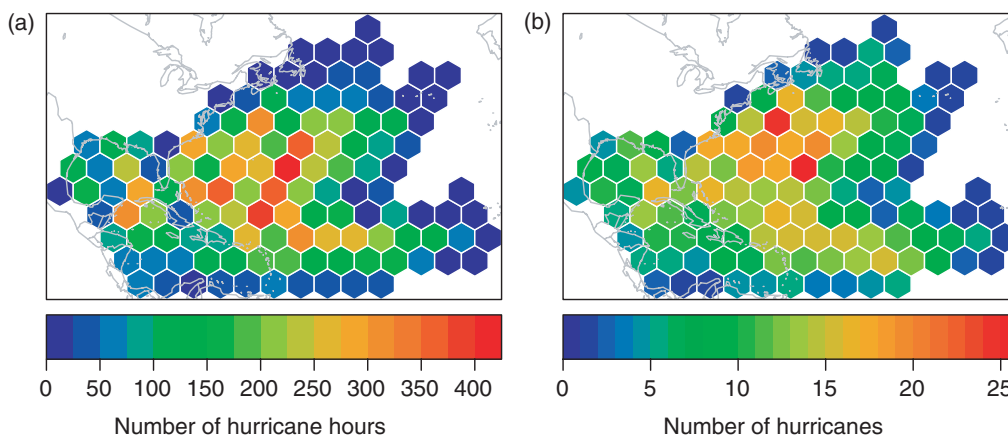


Figure 3. Hurricane hours and hurricane frequency. (a) The number of hurricane hours in each hexagon grid. (b) The hurricane frequency in each grid. The data are aggregated over the period 1986–2011.

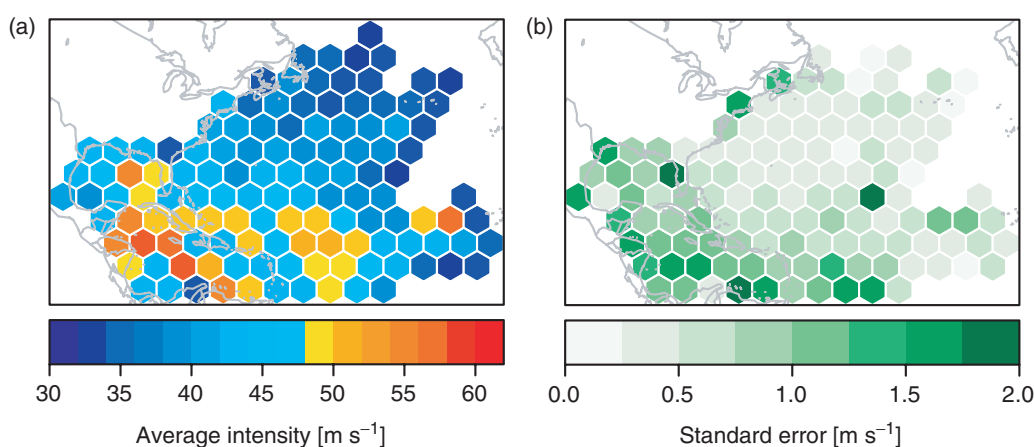


Figure 4. Mean hurricane intensity. (a) Average per hexagon wind speed (m s^{-1}). (b) Standard error (m s^{-1}). The data are aggregated over the period 1986–2011.

across the Greater Antilles where maximum intensification rates are relatively lower. This region is of particular note as this is where ocean temperatures are generally quite warm.

4. Average intensification

Here we examine the spatial variability of average intensification for two non-overlapping periods (1967–1985 and 1986–2011). Figure 7 shows the per hexagon mean intensification rates and the corresponding standard errors. A corridor of high intensification rates extends from the eastern Atlantic westward through the lesser Antilles and then northwestward into the Gulf of Mexico for both epochs. Some of the highest average intensifications occur over the southern Caribbean Sea where the standard errors are also fairly low. The standard errors on the mean intensifications are smaller than the standard errors on the mean intensity changes because decaying hurricanes are removed.

Spatial variability of intensification appears to be less in the later period. That is where there is greater spatial coherency (high values next to high values and low

values next to low values). This is verified by computing the spatial autocorrelation. The spatial autocorrelation is defined by Moran’s I, which is the slope of a regression of spatially lagged intensification onto the corresponding intensification (Moran, 1950). For each hexagon grid a spatially lagged intensification is computed by averaging the intensification values over the grid’s contiguous neighbours.

Moran’s scatter plots for the intensity change from the two periods are shown in Figure 8. The per grid intensification is plotted on the horizontal axis and the corresponding neighbourhood average intensification is plotted on the vertical axis. While both periods indicate positive spatial autocorrelation, the correlation is significantly larger in the latter. Moran’s I is 0.35 ± 0.054 (s.e.) over the period 1967–1985 but increases to 0.56 ± 0.049 (s.e.) for the period 1986–2011.

The cause of this increase in spatial autocorrelation of intensification is unknown. It might be related to improvements in estimating hurricane intensity but it seems that more precise intensity estimates would lead to greater along-track variation in intensity estimates and thus more spatial variability.

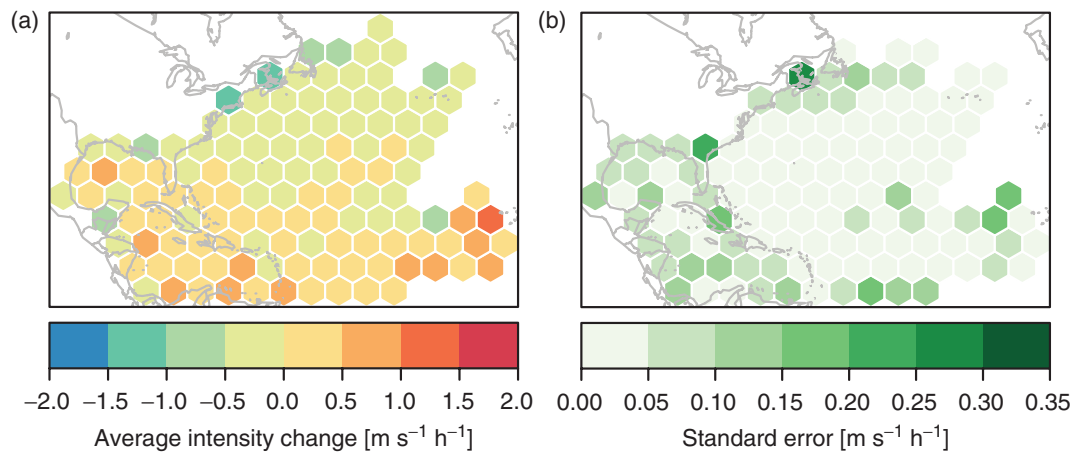


Figure 5. Mean hurricane intensity change. (a) Average per hexagon intensity change ($\text{m s}^{-1} \text{h}^{-1}$). (b) Standard error on the average intensity change ($\text{m s}^{-1} \text{h}^{-1}$). The data are aggregated over the period 1986–2011.

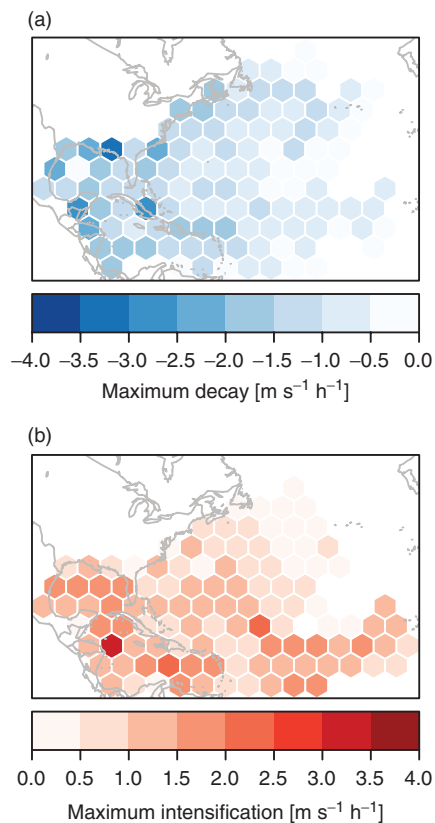


Figure 6. Maximum decay and intensification. (a) Maximum per hexagon decay ($\text{m s}^{-1} \text{h}^{-1}$). (b) Maximum per hexagon intensification ($\text{m s}^{-1} \text{h}^{-1}$). The data are aggregated over the period 1986–2011.

5. Intensity versus intensification

Finally we consider the relationship between intensity and intensification. Figure 9 is a scatter plot of the mean intensity *versus* mean intensification separated into the two periods. There is a positive relationship indicating that grids with high intensification tend to be paired with grids of high intensity and vice versa. However, the relationship is stronger and tighter during the later

period. This is indicated by the slope of the regression line where the intensification is regressed onto intensity.

The slope of the line in Figure 9(a) is $+0.010 \pm 0.0032 \text{ h}^{-1}$ (s.e.), indicating that for every 1 m s^{-1} increase in intensity, the intensification increases by $0.010 \text{ m s}^{-1} \text{ h}^{-1}$. The slope of the line in Figure 9(b) is larger at $+0.024 \pm 0.0032 \text{ h}^{-1}$ (s.e.). This increasing relationship between intensity and intensification is likely an artefact of better analysis of hurricanes over the most recent period. The enhanced infrared technique (EIR) of the Dvorak technique was introduced in 1984 (Dvorak, 1984). Knaff *et al.* (2010) notes that most of the reporting agencies had begun using the EIR Dvorak Technique in 1986. On the basis of this, and along with the work by (Kishtawal *et al.*, 2012), we chose to use the 1986–2011 time frame, and compare it to the previous time frame of 1697–1985. The Dvorak technique is detectable in the intensification rate, and this spatial consistency indicates that researchers need to be careful using data prior to 1984.

6. Summary

A neglected component of hurricane climatology is the spatial patterns associated with intensity change. Here we used a unique hourly interpolated version of HURDAT together with a novel spatial tessellation to examine the climatology of hurricane intensity change across the North Atlantic basin. Although the intensity values are positively skewed the change of intensity are symmetric about zero.

The distribution of the frequency (hurricane hours and number of hurricanes) and mean intensity of hurricanes over the period 1986–2011 are mapped across the hexagon grids. While the frequency of hurricanes is highest across the central part of the basin, regions of highest intensity are located farther south across the Caribbean. As expected, standard errors about the mean intensities are largest in regions adjacent to land. Grids having the largest increasing intensity values are also

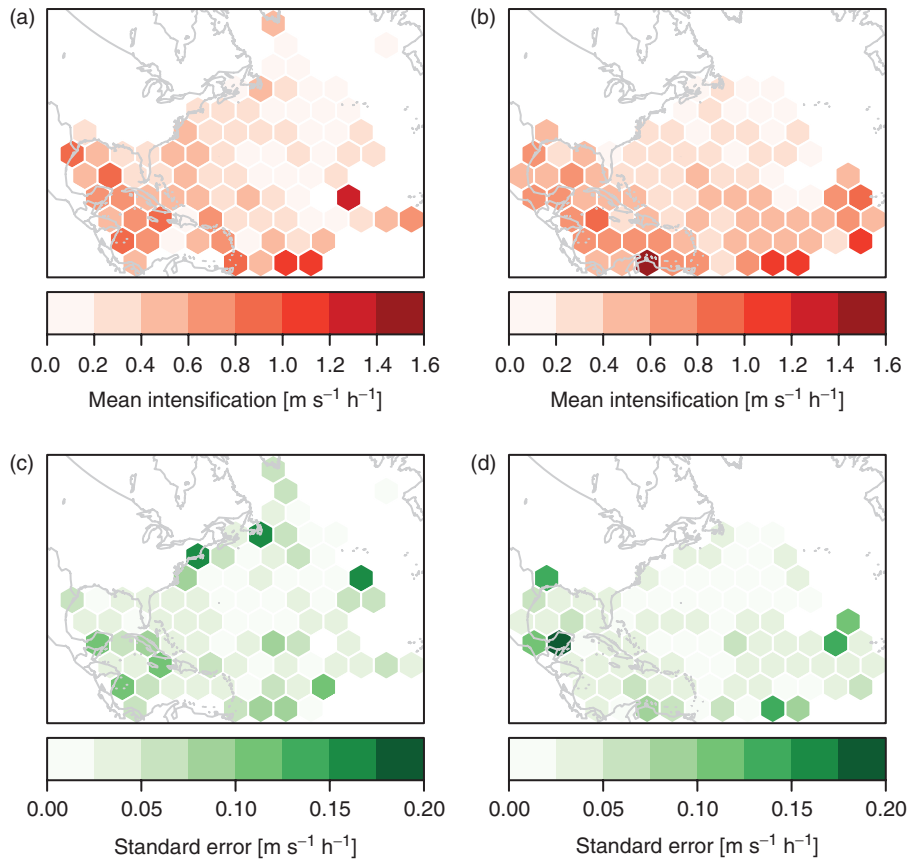


Figure 7. Average intensification and standard error. Average per hexagon intensification rate ($\text{m s}^{-1} \text{h}^{-1}$) for the periods (a) 1967–1985 and (b) 1986–2011. The corresponding standard errors are given in panels (c) and (d), respectively.

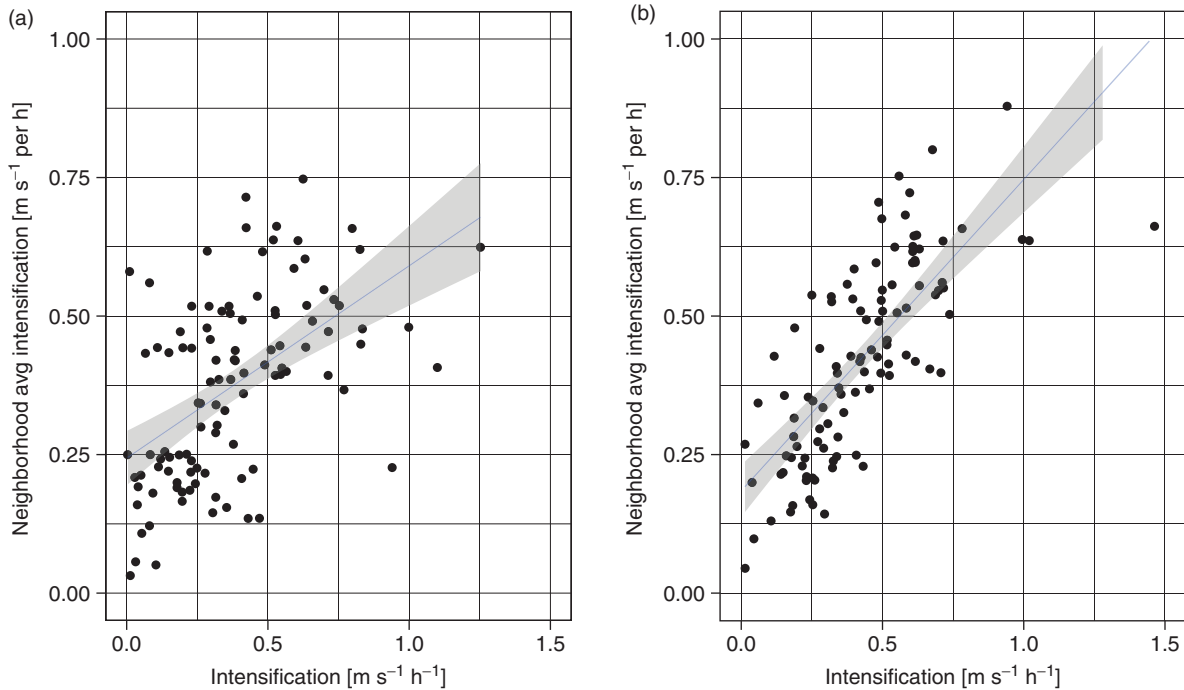


Figure 8. Moran's I for average intensification. Data from the periods (a) 1967–1985 and (b) 1986–2011. The regression line is shown in blue and the 95% confidence band on the slope is shown in grey.

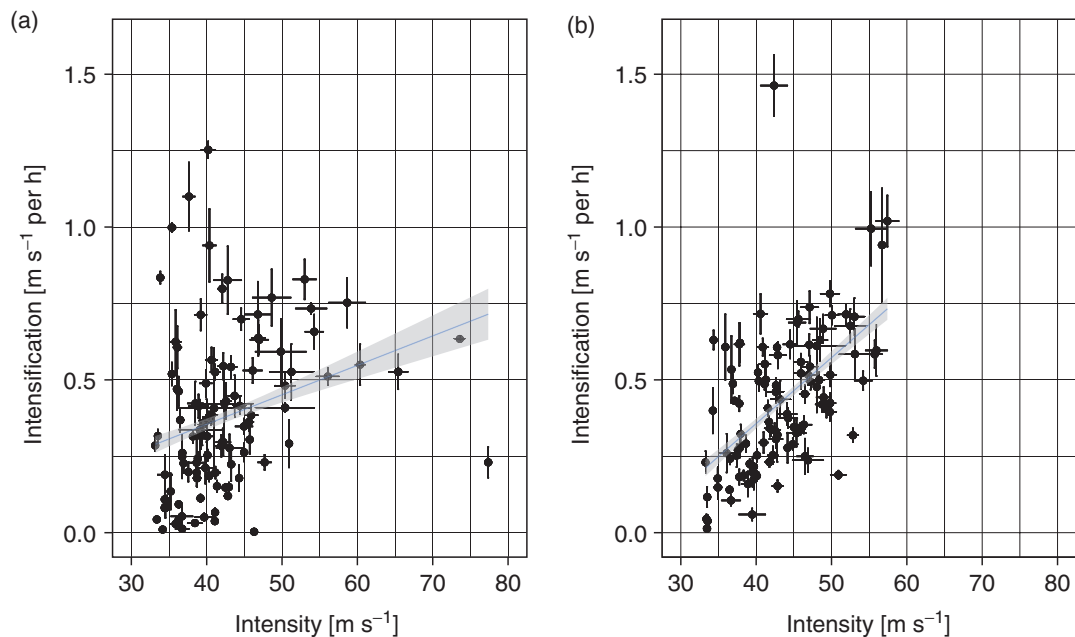


Figure 9. Intensity *versus* intensification. Data from the periods (a) 1967–1985 and (b) 1986–2011. The standard errors on the intensity and intensification are indicated by the crosses. The regression line is shown in blue and the 95% confidence band on the slope is shown in grey.

found primarily across the Caribbean Sea and the Gulf of Mexico.

The study compares the mean intensification (intensifying hurricanes only) between the periods 1967–1985 and 1986–2011. Highest mean intensification rates are found in the Gulf of Mexico and the Caribbean Sea, though the mean intensification is getting larger in the southeast portion of the basin. The analysis reveals greater spatial variability in intensification during the earlier epoch, which is quantified using a metric of spatial autocorrelation. The reason for this change is unknown but is likely due to the implementation of the Dvorak technique. Further, the statistical relationship between intensity and intensification appears to be getting stronger and tighter, likely due to the Dvorak technique. The Dvorak technique provided forecasters with a standardized way to forecast hurricanes. Once implemented in forecast offices, it is likely that the forecasting of hurricanes improved and became more consistent. The better spatial consistency shows that hurricane intensity data after 1984 are more reliable.

This study can help researchers determine specific regions to examine for rapid intensification. Further, this study can help emergency planners by showing which regions are more likely to see intensification. Finally, the methodology can be used to determine what role climatic features (e.g. El Niño) have on intensification.

The analysis and modelling were performed using the open-source R package for statistical computing. The code and data used to produce the figures in this paper are available from <http://www.rpubs.com/efraza28/6391>.

References

- Balling RC Jr, Cervený RS. 2006. Analysis of tropical cyclone intensification trends and variability in the north Atlantic basin over the period 1970–2003. *Meteorol. Atmos. Phys.* **93**: 45–51, DOI: 10.1007/s00703-006-0196-5.
- Dvorak VF. 1984. Tropical cyclone intensity analysis using satellite data. Technical Report, 45.
- Elsner J, Jagger T. 2013. *Hurricane Climatology: A Modern Statistical Guide Using R*. Oxford University Press: New York, NY.
- Elsner JB, Kossin JP, Jagger TH. 2008. The increasing intensity of the strongest tropical cyclones. *Nature* **455**: 92–95, DOI: 10.1038/nature07234.
- Elsner JB, Hodges RE, Jagger TH. 2012. Spatial grids for hurricane climate research. *Clim. Dynam.* **39**: 21–36, DOI: 10.1007/s00382-011-1066-5.
- Elsner JB, Strazzo S, Jagger TH, LaRow T, Zhao M. 2013. Sensitivity of limiting hurricane intensity to SST in the Atlantic from observations and GCMs. *J. Clim.* **26**: 5949–5957.
- Emanuel KA. 1988. The maximum intensity of hurricanes. *J. Atmos. Sci.* **45**(7): 1143–1155.
- Jarvinen BR, Neumann CJ, Davis MAS. 1984. A tropical cyclone data tape for the North Atlantic basin, 1886–1983: contents, limitations, and uses. Technical Memo. 22, NOAA NWS NHC.
- Kaplan J, DeMaria M. 2003. Large-scale characteristics of rapidly intensifying tropical cyclones in the north Atlantic basin. *Weather Forecast.* **18**: 1093–1108.
- Kaplan J, DeMaria M, Knaff JA. 2010. A revised tropical cyclone rapid intensification index for the Atlantic and eastern north pacific basins. *Weather Forecast.* **25**: 220–241.
- Kishtawal CM, Jaiswal N, Singh R, Niyogi D. 2012. Tropical cyclone intensification trends during satellite era (1986–2010). *Geophys. Res. Lett.* **39**(L10): 810, DOI: 10.1029/2012GL051700.
- Knaff J, Brown D, Courtney J, Gallina G, Beven J II. 2010. An evaluation of Dvorak technique-based tropical cyclone intensity estimates. *Weather Forecast.* **25**: 1362–1379.
- Moran PA. 1950. Notes on continuous stochastic phenomena. *Biometrika* **37**(1/2): 17–23.
- NHC. 2013. Glossary of NHC terms. <http://www.nhc.noaa.gov/aboutgloss.shtml>.
- Rozoff CM, Kossin JP. 2011. New probabilistic forecast models for the prediction of tropical cyclone rapid intensification. *Weather Forecast.* **26**: 677–689.
- Savitzky A, Golay MJE. 1964. Smoothing + differentiation of data by simplified least squares procedures. *Anal. Chem.* **36**(8): 1627–1639.